JOURNAL OF MATERIALS PROCESSING TECHNOLOGY 195 (2008) 248–254

journal homepage: www.elsevier.com/locate/jmatprotec

Nitrogen spray atomization of molten tin metal: Powder morphology characteristics

Renaud Metz[a,*], *Céline Machado*[a], *Mourad Houabes*[a], *Mazen Elkhatib*[a], *Mehrdad Hassanzadeh*[b]

[a] *Laboratoire Commun Lyon1-CNRS-SNPE Hydrazines et Procédés, UMR 5179, UCB Lyon 1, Bâtiment Berthollet (731) 3ème étage, 22 Avenue Gaston Berger, F-69622 Villeurbanne Cedex, France*
[b] *AREVA, 1340 Rue de Pinville, 34 965 Montpellier Cedex 2, France*

ARTICLE INFO

Article history:
Received 29 August 2006
Received in revised form
27 April 2007
Accepted 3 May 2007

Keywords:
Melt atomization
Tin powder

ABSTRACT

The gas atomization process used for metal powder production has been studied using a low melting point metal: tin. The influence of two experimental atomization parameters (gas flow rate and gas pressure) and the possibility to preview the particle mean diameter with the Lubanska equation are investigated. The ability of spray processing to control and produce well defined metal powders with both the desired particle size range and shape is discussed.

1. Introduction

The atomization process remains a good choice among the different methods of metal powder production due to the versatility, the quality and purity of the obtained powder, the control of its properties and the potential for mass production (Kuhn and Lawley, 1978).

The atomization process, as considered, in the present paper, is the starting step in a new production process of oxide ceramic powders. This new route named direct oxidation of a precursory alloy (DOPA) leads to a ceramic powder by total oxidation of a metallic alloy powder obtained by atomization (Metz et al., 2000, 2004). The oxide powder can then be pressed and sintered to obtain a bulk ceramic. The precursor metal alloys powders need to be accurately controlled in terms of chemical purity, morphology and particle size distribution. The aim of this study was to further the understanding of the atomization process as a basis for subsequent work on DOPA development and optimization.

A number of studies have been performed to relate the powder properties to the process parameters. Several authors have worked on gas atomization and shown the parameters influence on the final powders (Lagutkin et al., 2004; Özbilen, 2000; Goldaev et al., 1971; Gummeson and Ulf, 1972; Rao and Mehrotra, 1981; Date et al., 1967; Ünal, 1987; Helmersson et al., 1997; Tamura and Takeda, 1963; Beddow, 1977; Kim and Marshall, 1971). These works differ ones from the others by the nature of alloys, the atomization process, etc... It is therefore difficult to correlate them. However, the Lubanska equation (Lubanska, 1970), which is a modification of the Wigg equation (Wigg, 1964), is a typical semi-empirical correlation between the process parameters and the mass median particle, commonly used for metal atomization. It takes into account different experimental parameters such as gas and

* *Corresponding author*. Tel.: +33 4 72 44 83 27; fax: +33 4 72 43 12 91.
E-mail addresses: metz@univ-lyon.fr, metz@univ-lyon1.fr (R. Metz).
0924-0136/$ – see front matter © 2007 Elsevier B.V. All rights reserved.
doi:10.1016/j.jmatprotec.2007.05.006

metal flow rates, gas and metal kinematic viscosities, metal stream diameter and the Weber number. The mass median particle diameter as a function of the operating parameters is given by

$$d_m = d_t K \left[\frac{\nu_m}{\nu_g} \left(\frac{(1 + M/G)}{W_e} \right) \right]^{1/2} = d_t K \left[\frac{\nu_m (1 + M/G) \sigma S^2 \rho_g^2}{\nu_g G^2 \rho d_t} \right]^{1/2}$$

where d_m is the mass median particle diameter (m), d_t the diameter of the atomizer nozzle or the liquid stream diameter (m), ν_m and ν_g are, respectively, the kinematic viscosities of the molten metal and the gas ($m^2\,s^{-1}$), M and G are, respectively, the massic flow rates of the metal and the gas ($kg\,s^{-1}$). G' is the gas flow rate in L/min with $G = ((G'/1000)\rho_g)/60$, K is an experimentally determined constant for particular conditions of spray and liquid stream, in particular this constant is only available for one pressure, W_e the dimensionless Weber's number defined as $W_e = V^2 \rho d_t/\sigma$ where the gas velocity $V = G/S\rho_g$ and ρ the density of the metal ($kg\,m^3$), ρ_g the density of the atomizing gas ($kg\,m^3$), σ the surface tension of the liquid metal ($kg\,s^{-2}$) and S is the surface of the crown of the gas (m^2).

Two process parameters, mass flow rate and pressure of the atomizing gas, have been studied on tin metal. Indeed, few references are known on an annular configuration (Lubanska, 1970) and none with tin metal.

2. Experimental details

Tin granules of 99.9% purity were supplied by Fisher Labosi (France). The atomizing gas is nitrogen with a purity of 99.995%. The gas flowing path is illustrated in Fig. 1.

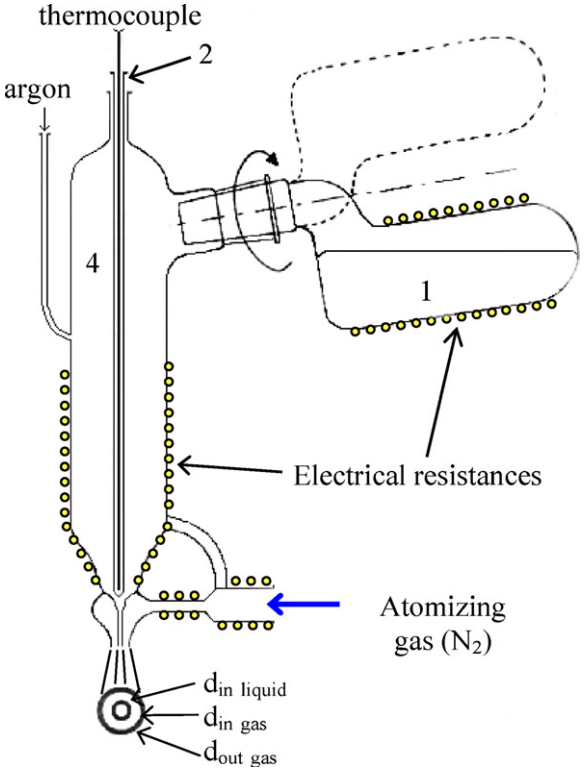

Fig. 1 – Experimental molten metal atomizer.

A fused silica container (item 1 in Fig. 1) is used to melt the metal. Once the metal is melted, the fused silica container is rotated (as indicated in Fig. 1) to transfer it into the atomiser proper, which is fully made in fused silica too. To reduce uncontrolled oxidation, experiments are conduced under argon flow. The fused silica container (item 1) and the atomiser metal recipient (item 4) parts 1 are heated by rolled up electric resistances around the silica surface (3). The tube 2 is used to blank the nozzle so that atomization can start at the desired time. Moreover, there is a thermocouple inside the tube to indicate the temperature of the liquid metal. The atomizing gas (nitrogen) enters at the right of the system and atomises the liquid metal by a crown of spray around the nozzle. The metal droplets are quenched into cold water or liquid nitrogen to obtain a metallic powder.

The dried atomised particles were sieved according to ASTM standard and weighted for size distribution analysis. A sample of known weight is passed through a set of sieves of known mesh sizes. They are mechanically vibrated for a period of time of 2 min. The weight of powder retained on each sieve is measured and converted into a percentage of the total powder sample.

The phases present in the powders were identified by X-ray diffractometry (XRD). The X-ray measurements were conducted in a Siemens diffractometer model using Cu $K\alpha 1$ radiation with a wavelength $\lambda = 0.154$ nm. Powder XRD were determined in the $2\theta = 5$–90° range with a resolution of 0.02° and a time step of 1 s.

Characterization of the powder morphology was carried out using a Scanning Electron Microscope (SEM) Hitachi S800.

3. Results and discussion

3.1. *Particle size distribution of atomized tin powders*

The raw data of the particle size distribution, established by mechanical sieving, is given in Table 1. The size distribution is also depicted by the histogram and by the cumulative fraction (Fig. 2).

The statistical values calculated from the experimental data are the median particle size (x_{med}) which is the value corresponding to 0.5 on the cumulative fraction curve, the average

Table 1 – Particle size distribution (experimental conditions: pressure of 2 bar and gas flow rate of 30 L/min)

Size (μm)	Mass (g)	Fraction	Cumulative fraction
10	0	0	0
20	0.1319	0.0033	0.0033
30	0.7973	0.0200	0.0233
40	2.3529	0.0591	0.0824
63	6.0944	0.1530	0.2354
80	4.8701	0.1223	0.3577
125	9.7853	0.2457	0.6034
250	13.0859	0.3286	0.9320
500	2.7091	0.0680	1

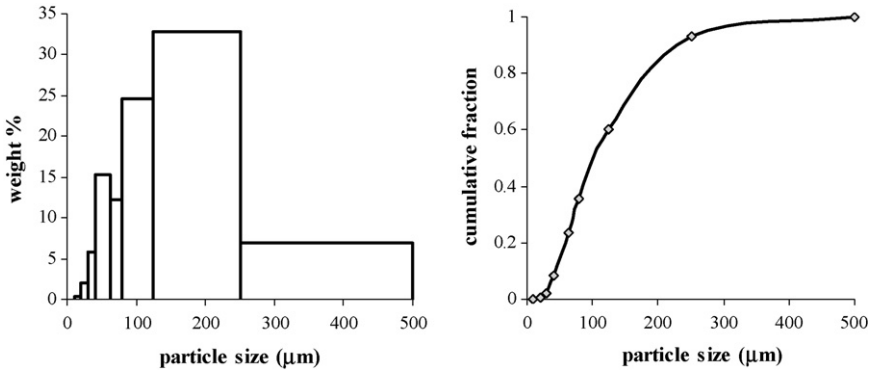

Fig. 2 – Particle size distribution data: histogram and cumulative fraction representations (experimental conditions: pressure of 2 bar and gas flow rate of 30 L/min).

particle size (x_{ave}), the standard deviation (σ), the skewness which determines the lack of symmetry around the center of the distribution and the kurtosis corresponding to a measure for peakedness.

For the same experimental conditions (pressure of 2 bar and gas flow rate of 30 L/min), these values are summarized in Table 2.

Table 2 – Statistical values for particle size distribution (experimental conditions: pressure of 2 bar and gas flow rate of 30 L/min)

Characteristic	Value
x_{med}	102 μm
x_{ave}	131.5 μm
σ	86.7
Skewness	1.3
Kurtosis	1.6

3.2. *Particle size distribution modelling*

The particle size distribution may be approximated by statistical functions. The most commonly used are the power law ($F(x) = 1 - (x/x_{min})^{-a}$), exponential law

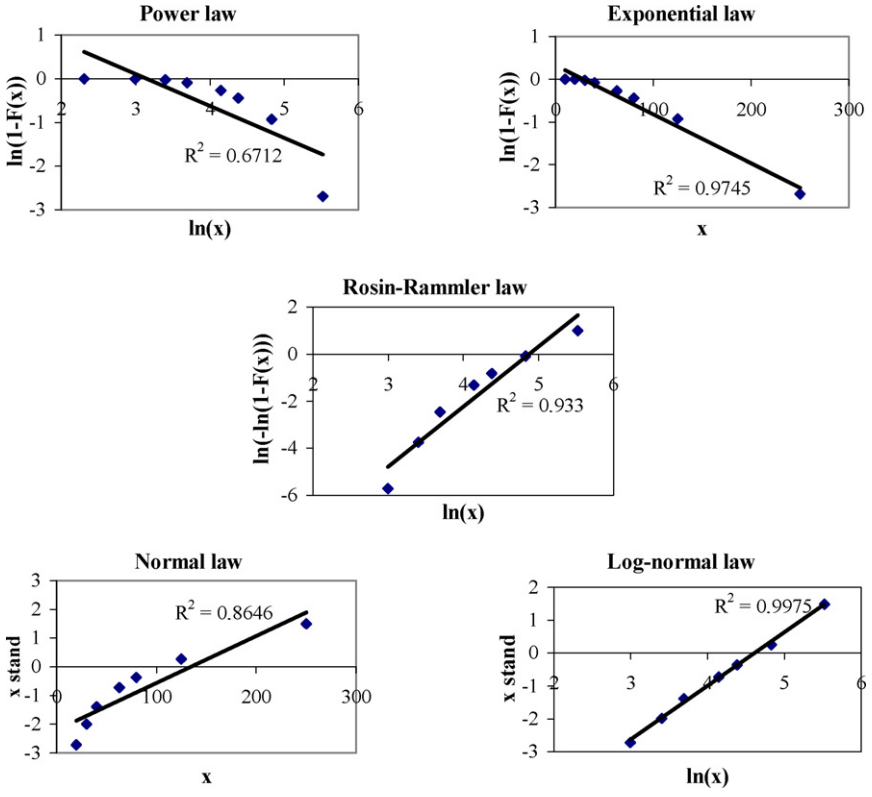

Fig. 3 – Tests for approximation of particle size distribution to statistic laws (experimental conditions: pressure of 2 bar and gas flow rate of 30 L/min).

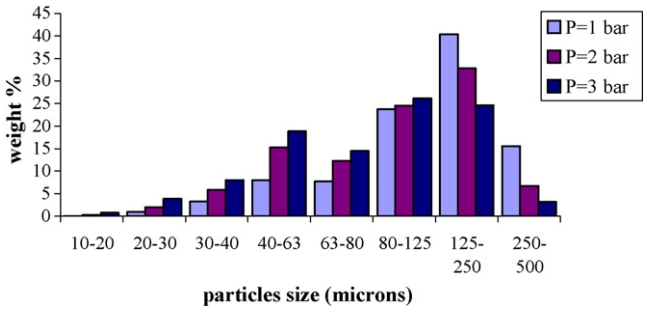

Fig. 4 – Influence of the atomising gas pressure on particle size: histogram (experimental conditions: pressure of 1, 2 and 3 bar and gas flow rate of 30 L/min).

Table 3 – Characteristic values for particle size distribution: influence of gas pressure (experimental conditions: pressure of 1, 2 and 3 bar and gas flow rate of 30 L/min)

	x_{med}	x_{ave}	σ	Skewness	Kurtosis
P = 1 bar	140	170	102	0.9	−0.07
P = 2 bar	102	131	87	1.3	1.6
P = 3 bar	85	109	73	1.5	3.1

($F(x) = 1 - \exp(-(x - x_{min})/x_0)$), the normal law, the log-normal law and the Rosin–Rammler law ($F(x) = 1 - \exp(-(x/x_0)^a)$) (Verheijen, 2001).

These five functions have been tested to check their suitability to the experimental size distribution.

The results summarized in Fig. 3 show that the size distribution of the atomized powders, in agreement with other studies (Ünal, 1987; Kim and Marshall, 1971; Juarez-Islas et al., 1999), fit best the log-normal law ($R^2 > 99\%$) (the *R*-squared-values of power, exponential, Rosin–Rammler and normal law are respectively: 0.67, 0.97, 0.93 and 0.86).

3.3. *Influence of atomizing gas pressure*

The influence of atomizing gas pressure on particle size distribution has been studied at three levels (1, 2 and 3 bar) with a constant gas flow rate of 30 L/min. The distribution evolution is represented by the histogram and cumulative fraction as shown on Figs. 4 and 5, respectively.

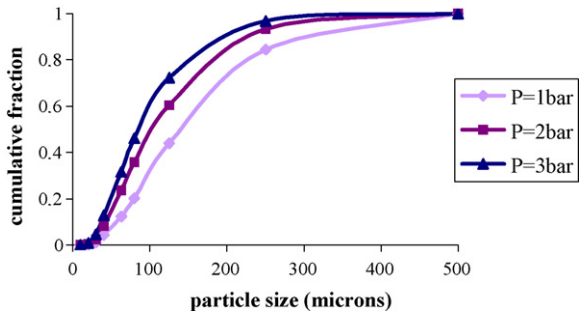

Fig. 5 – Influence of the atomising gas pressure on particle size: cumulative fraction (experimental conditions: pressure of 1, 2 and 3 bar and gas flow rate of 30 L/min).

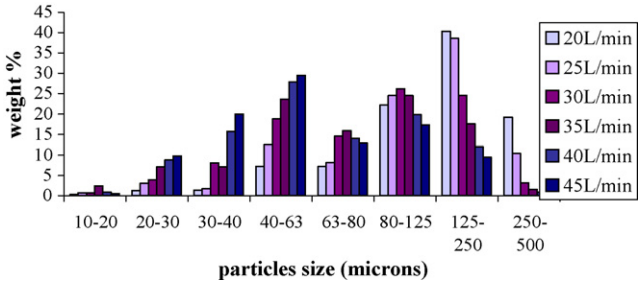

Fig. 6 – Histogram for particle size distribution as a function of the atomising gas flow rate from 20 to 45 L/min (P = 3 bar).

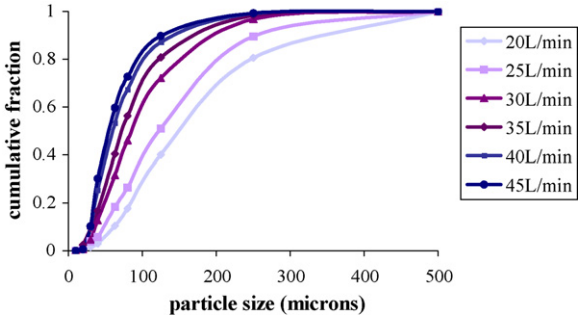

Fig. 7 – Cumulative fraction for particle size distribution in function of the atomising gas flow rate from 20 to 45 L/min (P = 3 bar).

The characteristic statistical (x_{med}, x_{ave}, σ, skewdness and kurtosis) values are given in Table 3. The results show that pressure variation has a strong influence on the statistical parameters of the distributions: the mass median diameter, average diameter and standard deviation decrease with increasing pressure. Other studies (Helmersson et al., 1997; Tamura and Takeda, 1963) confirm that increasing the pressure leads to decrease median powder particle size.

3.4. *Influence of gas flow rate*

Figs. 6 and 7 show the influence of the gas flow rate on the particle size distribution represented by the histogram and cumulative fraction. Table 4 summarises the different characteristic values obtained during the present experimental work.

Table 4 – Characteristic values for particle size distribution: influence of gas flow rate (experimental conditions: pressure of 3 bar and gas flow rate from 20 to 45 L/min)

	x_{med}	x_{ave}	σ	Skewness	Kurtosis
20 L/min	149	181	107	0.7	−0.5
25 L/min	123	150	95	1.1	0.7
30 L/min	85	109	73	1.5	3.1
35 L/min	72	92	63	1.7	4.2
40 L/min	60	78	55	2	5.9
45 L/min	55	72	52	2.3	7.6

Table 5 – Comparison between the experimental (d_{exp}) and calculated (d_{cal}) mean diameters

Flow rate (L min^{-1})	P = 1 bar		P = 2 bar		P = 3 bar	
	d_{exp} (μm)	d_{cal} (μm)	d_{exp} (μm)	d_{cal} (μm)	d_{exp} (μm)	d_{cal} (μm)
20	200	206	168	158	149	143
25	174	159	148	128	123	106
30	140	139	102	99	85	85
35	–	–	87	86	72	71
40	–	–	–	–	60	61
45	–	–	–	–	55	54

Consistent with other studies (Kim and Marshall, 1971; Juarez-Islas et al., 1999), the present results demonstrate that the mass median diameter x_{med} decreases when increasing the atomizing gas flow rate. The average diameter x_{ave} shows similar behaviour. The spread of the size, represented by the standard deviation, σ, increases also for low atomizing gas flow rates indicating that relatively a higher proportion of large particles are present in such powders.

3.5. *Correlation between the Lubanska equation and experimental data*

Table 5 compares the experimental data with the calculated values for different gas flow rates and gas pressures. The experimental and calculated mean diameters are in good agreement. This formula can then estimate the particle mean diameter for different values of gas flow rates and pressures.

It is now interesting to verify if this mathematical function confirms the experimentally determined influence of these two parameters on the mean diameter of the powder particles. The Lubanska formula suggests that the mean particle diameter decreases with increasing the atomizing gas flow rate: $d_m = d_t K[(\nu_m/\nu_g)(S^2\sigma\rho_g^2/G^2\rho d_t)(1 + M/G)]^{1/2}$. It confirms the experimental data given in Figs. 4 and 5 and in Table 2.

3.6. *Study of particle morphology*

The influence of the quenching liquid (cold water or liquid nitrogen) on the form of the metallic particles has been studied. The SEM photographs show that particles quenched in liquid nitrogen have a more spherical or oblong shape and are smoother (Fig. 8). Moreover, it will be seen on the next SEM photograph that the sphericity of the particles increase with the decrease of the size distribution range of the powder and that the powder shape is more spherical and regular (Fig. 9). These observations may be interpreted on the basis of the difference between the specific heat capacity and thermal conductivity between water and nitrogen which are 0.61 W m^{-1} K^{-1} versus 0.13 W m^{-1} K^{-1} and 4.18 J g^{-1} K^{-1} versus 2.04 J g^{-1} K^{-1}, respectively. A drop of metal falling into liquid nitrogen should cool slower than in a water medium. Moreover, the spherical shape may find its origin by the creation of a film of nitrogen gas wrapping the drops of liquid metal during the quench operation.

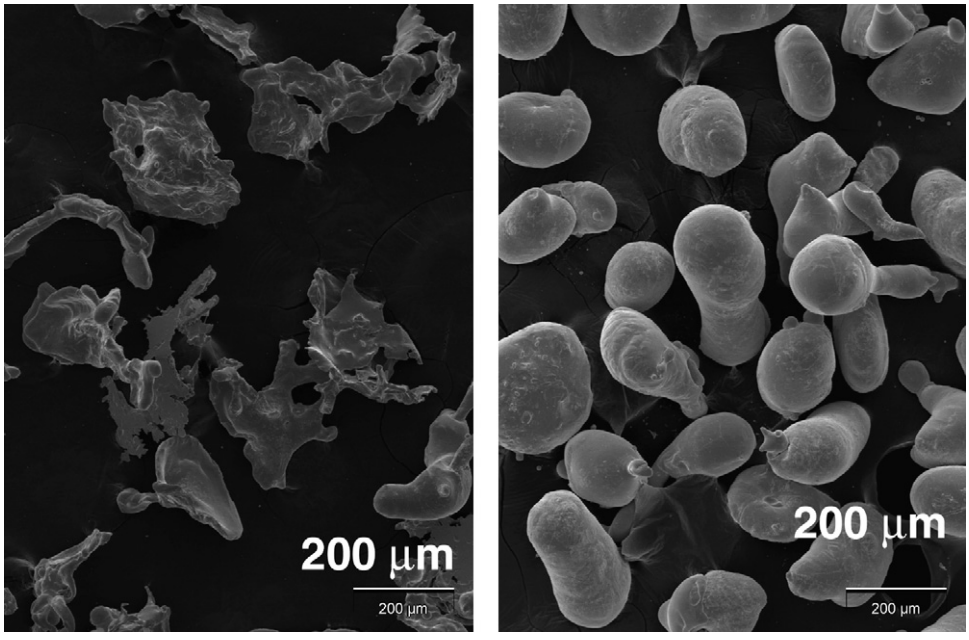

Fig. 8 – Influence of the quenching liquid on the particle morphology: on the left, particles quenched into cold water and on the right, particles quenched into liquid nitrogen.

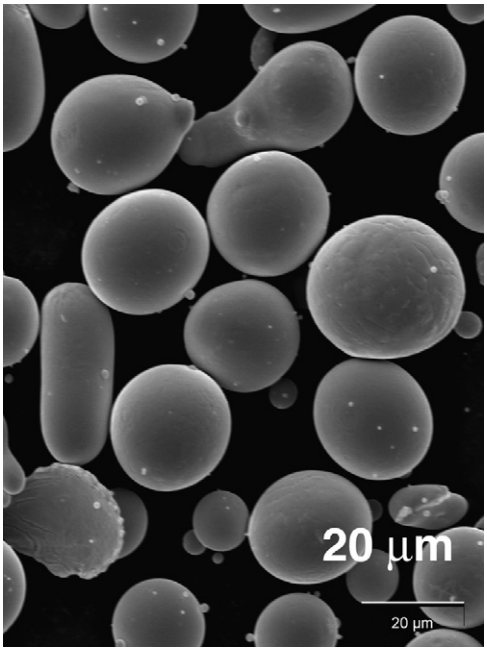

Fig. 9 – Morphology of particles of 20–30 μm (particles quenched into liquid nitrogen).

A polished cross-section of these metal particles have been examined to assess the powder internal densification. The powder particles were mounted into a polymeric resin and the resin was polished until the particles are cut around the middle. An example of a SEM image is shown in Fig. 10. The surface of this cross-section presents some scratches due to burnishing. It can be noted that the particle is fully densified and does not present any apparent macroscopic porosity.

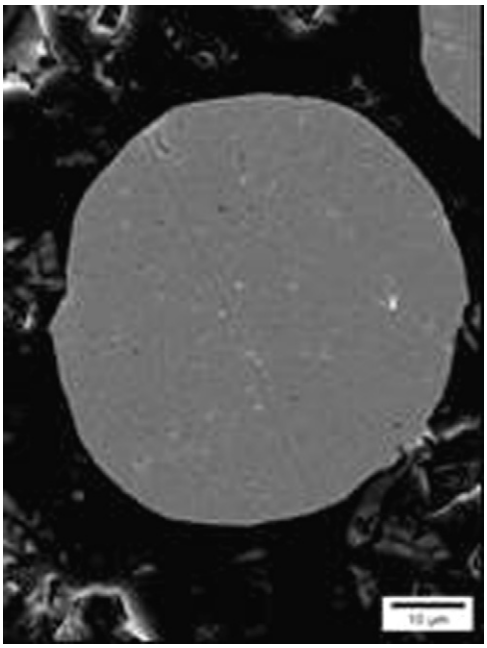

Fig. 10 – SEM of a cross-section of a tin particle (40–63 μm).

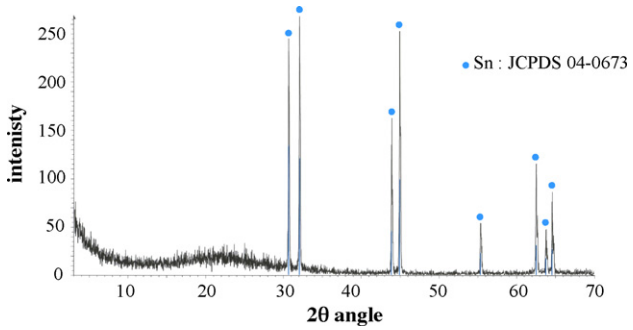

Fig. 11 – X-ray diffraction diagram of atomised tin powder.

3.7. *Analysis of the purity of the obtained powders*

X-ray diffraction analysis has been carried out to check the absence of foreign phases. Pollution could indeed arise from the interaction between the molten metal and the atomizing gas or the quenching media (cold water or liquid nitrogen) inducing the formation of nitrides or oxides.

Fig. 11 shows a typical PXRD pattern. In the limiting detection of 2% of the X-ray, it was not possible to detect any by-product as a consequence of a reaction between molten tin and its surrounding.

4. Summary

This study gives a full characterisation of atomised tin. Particle size distribution with histogram and cumulative fraction representations, with location, width, asymmetry and peakedness descriptors, and the approximation of the distribution by the log-normal function and with the phase and morphology have been determined.

These atomization experiments confirm the strong influence of two processing variables (gas pressure and gas flow rate) on particle size distribution. It has been shown that increasing gas flow rate or gas pressure leads to a decrease of median particle size and width of the distribution measured by standard deviation.

The experimental size distributions have been successfully approximated by a log-normal law after comparison with other commonly used mathematical functions.

In the experimental range study, the Lubanska formula has been successfully applied to tin metal powders obtained by atomization through an annular nozzle.

Moreover, the influence of the quenching liquid on the particle morphology has been demonstrated and liquid nitrogen seems to be the preferable choice to make spherical particles.

Moreover, powders obtained by atomization do not show any pollution due to this process.

REFERENCES

Beddow, J.K., 1977. The production of metal powders by atomisation, Powder Monographs in Science and Technology. A.S. Goldberg.

Date, U.R., Tendolkar, U.R., Gangadar, S., Vartak, M.N., 1967. Statistical interpretation of metal atomization. Int. J. Powder Metall. (New York) 3 (2), 49–55.
Goldaev, I.P., Motornenko, A.P., Shevchenko, A.P., Lastivnyak, Yu.A., 1971. Gas-jet atomization of liquid metals and alloys. Poroshkovaya Metallurgiya (Kiev) 11 (2), 9–13.
Gummeson, P., Ulf, P., 1972. Modern atomizing techniques. Powder Metall. 15 (29), 67–94.
Helmersson, G., Hede, A., Johannesson, T., Bergman, B., Hallen, H., 1997. On the control of powder-size distribution in full-scale gas atomization of nickel-based alloys. Scand. J. Metall. 26, 93–101.
Juarez-Islas, J., Zhou, Y., Lavernia, E.J., 1999. Spray atomization of two Al–Fe binary alloys: solidification and microstructure characterization. J. Mater. Sci. 34, 1211–1218.
Kim, K.Y., Marshall, W.R., 1971. Drop-size distributions from pneumatic atomizers. AIChE J. 17, 575–584.
Kuhn, H.A., Lawley, A., 1978. Powder Metallurgy Processing, New Techniques and Analyses. Academic Press (Ed.).
Lagutkin, S., Achelis, L., Sheikhaliev, S., Uhlenwinkel, V., Srivastava, V., 2004. Atomization process for metal powder. Mater. Sci. Eng. A 383 (Issue 1), 1–6.
Lubanska, H., 1970. Correlation of spray ring data for gas atomization of liquid metals. J. Metals 22 (2), 45–49.
Metz, R., Delalu, H., Vignalou, J.R., Achard, N., Elkhatib, M., 2000. Electrical properties of varistors in relation to their true bismuth composition after sintering. Mater. Chem. Phys. 63, 157–162.
Metz, R., Machado, C., Hassanzadeh, M., Puyané, R., 2004. Direct oxidation of an alloy precursor. Complete oxidation of bismuth and zinc powder. J. Electroceram. 13, 825–827.
Özbilen, S., 2000. Studies of gas atomization of aluminium, copper, zinc, tin and aluminium alloy powders. Metal Powder Report 55 (6), 36.
Rao, K.P., Mehrotra, S.P., 1981. Effect of process variables on atomization of metals and alloys. Modern Dev. Powder Metall. 12, 113–130.
Tamura, K., Takeda, T., 1963. A study on production pf copper powder by atomization. Trans. Natl. Res. Inst. Metals 5, 252–256.
Ünal, A., 1987. Effect of processing variables on particle size in gas atomization of rapidly solidified aluminium powders. Mater. Sci. Technol. 3, 1029–1039.
Verheijen, P.J.T., 2001. Statistical Distributions in Particle Technology. Particle Technology Course, Department of Chemical Engineering, Technical University Delft, The Netherlands.
Wigg, L.D., 1964. Drop-size prediction for twin-fluid atomisers. J. Inst. Fuel 11, 46–52.